# Tribological behavior of three silicon nitride ceramics in dry sliding contact against Inconel 718 in a wide range of velocities

Bin Zhao[a], Iyas Khader[b,a], Rahul Raga[a], Ulrich Degenhardt[c], Andreas Kailer[a]

[a] Fraunhofer Institute for Mechanics of Materials IWM, Wöhlerstraße 11, 79108 Freiburg, Germany

[b] Department of Industrial Engineering, German-Jordanian University, P. O. Box 35247, 11180 Amman, Jordan

[c] FCT Ingenieurkeramik GmbH, Gewerbepark 11, 96528 Frankenblick, Germany

## Abstract

Silicon nitride based ceramic tools have been successfully applied in high speed machining of nickel-based alloys. In this study, three silicon nitride material systems with different intergranular glassy phase content were used to study the tribological behavior of silicon nitride in dry sliding against Inconel 718 in order to evaluate their potential suitability for cutting tool materials. The tribological properties at sliding velocities ranging from 1 m/s to 20 m/s were investigated. The mechanical and microstructural properties of ceramics were considered, and the wear mechanisms were analyzed. The results showed that the wear of the ceramics has a positive correlation with hardness for sliding velocities below 5 m/s. With increasing sliding velocity, a tribochemical layer consisting of an oxide layer and a diffusion layer forms at the interface, resulting in increasingly higher wear of the ceramic. The formation of a tribochemical layer showed a correlation with the amount of the intergranular glassy phase in the material; the higher its amount the more prone the silicon nitride ceramic was found to form a tribochemical layer.

Keywords: Silicon nitride; Inconel 718; tribochemical wear; dry sliding; glassy phase

## 1 Introduction

Silicon nitride-based ceramic tools are often applied in dry and high-speed machining of nickel-based alloys [1]. Many researchers have made efforts to improve the cutting performance of silicon nitride-based ceramic tools by adding a toughening phase [2, 3] or changing the tool structure [4]. However, severe flank wear lowering tool life is still an important reason restricting its wide application in high-speed machining [5].

Generally, the wear resistance of ceramics may be increased by improving the mechanical properties [6]. The wear of ceramic-based tools dominated by mechanical wear (e.g., sliding wear and abrasion) is known to be dependent on both the fracture toughness and the hardness [7, 8]. Nevertheless, Doğan et al. [9] have found that for $Si_3N_4$ ceramic tool material toughened by SiC whisker, the wear resistance dropped despite an increase in hardness and fracture toughness. Park et al. [10] reported the same

phenomenon in $Si_3N_4$ whisker toughened SiAlON. Even though the mechanical properties were improved by whiskers, thermal tensile residual stresses concentrated at grain boundaries resulted in the detachment of the whiskers during the friction process; thus, resulting in high wear rates. Hence, the wear resistance of ceramics can be influenced by altering both the mechanical properties and the microstructure. Generally, the hardness of silicon nitride can be increased by refining the grain size or decreasing the glassy phase content. This results in improving its wear resistance in cases in which wear is mainly governed by mechanical processes [11]. Kurama et al. found that SiAlON ceramics with stronger interfaces exhibit lower wear rates in sliding contact against 100Cr6 bearing steel [12].

In high-speed machining of Inconel 718, the wear of ceramic tools can be accelerated due to diffusional wear (due to the diffusion of silicon) caused by high cutting temperature [13]. Bhattacharyya et al. found that a diffusion zone formed between the SiAlON ceramic tool and Inconel 901 above a speed of 185 m/min [14]. Addhoum and Broussaud studied the interaction between ceramic cutting tools and nickel-based alloys and also found it to be governed by diffusion of silicon that occurred at temperatures above 1100 °C [15]. Renz et al. [16] and Khader et al. [17] studied the tribological behavior of silicon nitride and SiAlON ceramics in sliding contact against Inconel 718. The authors found that the tribochemical wear caused by diffusion became dominant at high sliding velocities (up to 25 m/s), thus, promoting and increasing wear rate.

Generally, the wear resistance of silicon nitride related to mechanical wear increases with refining grain size, decreasing glassy phase content and strengthening the grain boundary. During high-speed machining, excessive contact temperatures accelerate diffusional wear. However, it is still unclear how the microstructure affects the wear of silicon nitride-based ceramic tools in machining nickel-based alloys. The study investigates the tribological behavior of three silicon nitride-based material systems with different intergranular glassy phase content. Dry sliding contact tests of silicon nitride against Inconel 718 were carried out over a wide range of sliding velocities. The work aims at providing fundamental knowledge indispensable in developing novel silicon nitride based ceramic tools for application in high-speed machining of nickel-based alloys.

## 2 Experimental

Three different grades of silicon nitride ceramics (SN-GP Low Cost, SN-GP High End and SN-PU High Purity) were tested in dry sliding contact against Inconel 718 at room temperature using a pin-on-disc experimental setup. SN-GP Low Cost (SN-GPLC) and SN-GP High End (SN-GPHE) are gas pressure sintered, whereas SN-PU High Purity (SN-PUHP) is a hot pressed grade. The three silicon nitride ceramics exhibit different mechanical and microstructural properties listed in Table 1 and Table 2, respectively. The

temperature depended flexural strength and Weibull modulus are plotted in Fig. 1a. High temperature four point bending tests were performed in accordance with DIN EN 843-2 and DIN EN 843-1. Temperature dependent thermal conductivity and specific heat of the ceramics are shown in Fig. 1b. Scanning electron microscope (SEM) images of the microstructure is shown in Fig. 2. On the left side of each SEM micrograph in Fig. 2, a bar chart shows the relative atomic content (at. %) of the elements in each material. As can be seen in Fig. 2, the intergranular glassy phase content of the three ceramics decreases such that it is highest for SN-GPLC and lowest for SN-PUHP, whereas a gradual refined in grain size was achieved so that SN-GPLC has the largest typical crystal length and SN-PUHP exhibits the smallest (Table 2). The chemical composition of Inconel 718 is listed in Table 3.

Table 1 Properties of the ceramics

| **Materials** | **Temperature** | **SN-GPLC** | **SN-GPHE** | **SN-PUHP** |
|---|---|---|---|---|
| Elastic modulus (GPa) | 25 °C | 292 | 306 | 318 |
| | 1000 °C | 210 | 240 | 275 |
| Density (g/cm$^3$) | 25 °C | 3.25 | 3.22 | 3.21 |
| Hardness HV20 (GPa) | 25 °C | 14.3 | 15.8 | 15.9 |
| Fracture toughness (MPa·m$^{1/2}$) | 25 °C | 5.9 | 6.1 | 5.1 |

Table 2 Microstructural properties of the ceramics

| **Materials** | **SN-GPLC** | **SN-GPHE** | **SN-PUHP** |
|---|---|---|---|
| Max. defect size (µm) | 60 | 40 | 5 |
| Max. crystal length (µm) | 8 | 20 | 8 |
| Typical crystal length (µm) | 5 | 4-15 | 1-4 |
| Crystal aspect ratio | 5 | 8 | 3 |

Table 3 Chemical composition of Inconel 718 [18]

| **Element** | **C** | **Si** | **Mn** | **Ni** | **Co** | **Cr** | **Al** | **Ti** | **Mo** | **Nb** | **Cu** | **Fe + others** |
|---|---|---|---|---|---|---|---|---|---|---|---|---|
| Content (wt.%) | 0.036 | 0.19 | 0.05 | 51.17 | <1.0 | 19.02 | 0.60 | 1.00 | 3.07 | 5.01 | 0.02 | Balance |

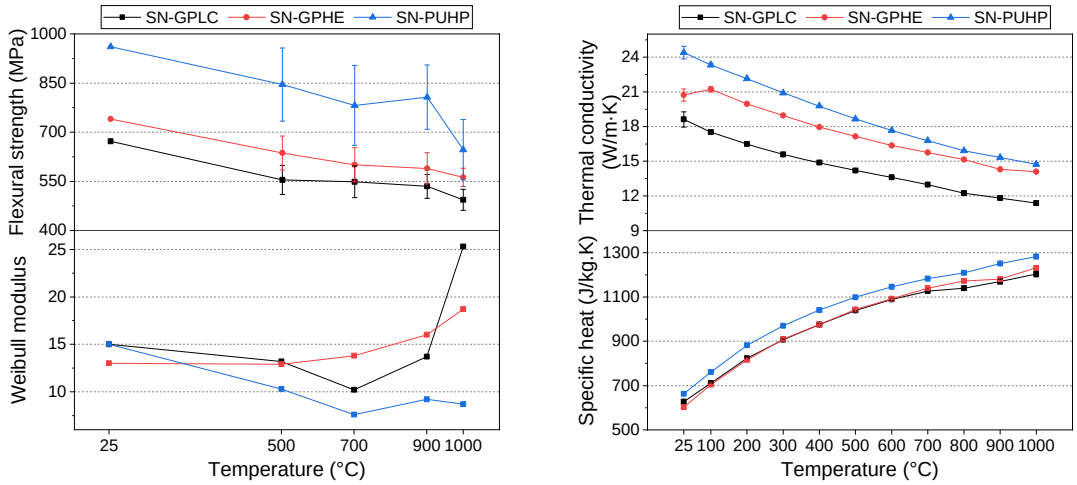


(a) (b)

Fig. 1 Temperature dependence of (a) flexural strength and Weibull modulus, and (b)thermal conductivity and specific heat of the ceramics; data points indicate mean values and error bars indicate standard deviation

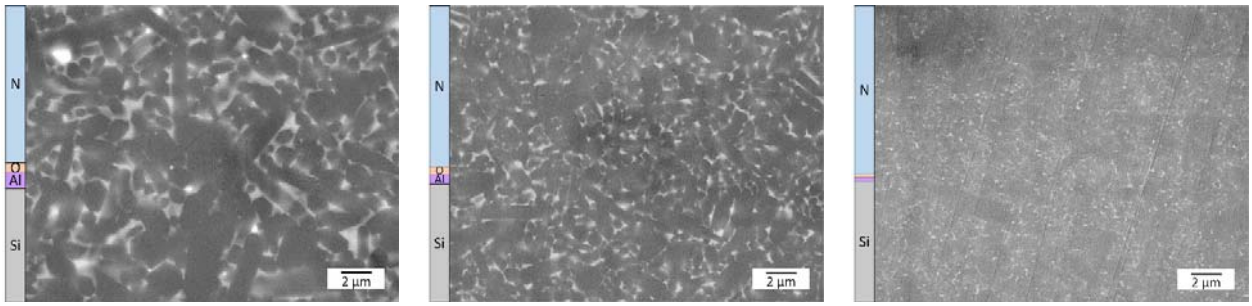


(a) (b) (c)

Fig. 2 SEM images showing the microstructure of the ceramic materials (a) SN-GPLC, (b) SN-GPHE, and (c) SN-PUHP

The ceramic pin with a CNGN-type insert geometry is shown in Fig. 3a. The test setup is shown in Fig. 3b. The ceramic sample was fixed into the tribometer using a special fixture designed to withstand the tangential forces emerging from dry sliding.

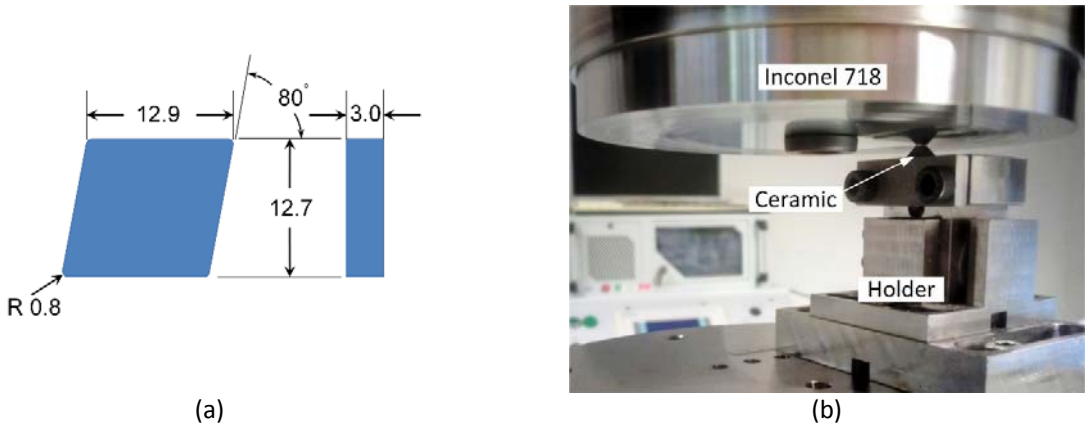


(a) (b)

Fig. 3 (a) ceramic sample geometry and (b) sliding-contact experiment set-up.

The contact between the ceramic pin and the metallic disk creates a 3 mm line contact. The applied normal force was 100 N and the sliding speed was in the range between 1 m/s and 20 m/s. The applied load of 100 N corresponds to an initial Hertzian line contact pressure of 1.32 GPa. This value is comparable with applied loads at cutting edges of machining tools [16]. A sliding distance of 2000 m was maintained for all tests. At least two repeat tests were carried out. The wear volume was calculated by measuring the wear land (width of the contact surface) of each ceramic sample using light microscopy. The coefficient of friction (COF) was recorded by the tribometer. The experimental parameters are listed in Table 4.

Table 4 Experimental parameters of the sliding-contact experiments

| | |
|---|---|
| Normal applied load (N) | 100 |
| Sliding velocity of the ceramic samples (m/s) | 1, 5, 10, 20 |
| Sliding distance (m) | 2000 |
| Temperature (°C) | Ambient temperature |
| Lubricant | Dry sliding |
| Atmosphere | Air |

Ceramographic cross-sectional analysis was conducted on the used samples. SEM and energy-dispersive X-ray spectroscopy (EDX) were carried out to investigate any microstructural and/or chemical alteration taking place in the tested samples.

# 3 Results

## 3.1 Experimental results

The mean value of the coefficient of friction (COF) plotted against the sliding velocity is shown in Fig. 4. For the three ceramics, the mean values of COF are almost identical at the same sliding velocity. The COF decreases in a similar trend with increasing sliding velocity. The COF decreases from $\mu$=0.57 at 1 m/s to $\mu$=0.20 at 20 m/s.

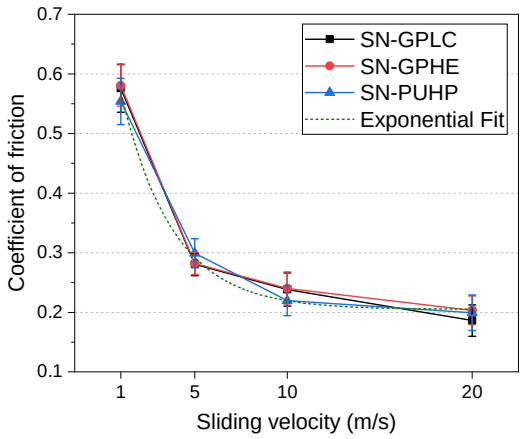


Fig. 4 Mean value of COF plotted against sliding velocity

The sliding velocity dependence of the wear volume is plotted in Fig. 5. For all three ceramics, the wear volume initially decreases and then increases with increasing sliding velocity. At 1 m/s, the wear volume of SN-GPHE and SN-PUHP is very close and smaller than that of SN-GPLC. At 5 m/s, all three ceramics show almost the same wear volume. Above 10 m/s, the wear volume of SN-GPHE becomes similar to that of SN-GPLC and greater than that of SN-PUHP. SN-PUHP shows the best wear resistance among three ceramics throughout the sliding velocity range. The lowest wear volume of SN-PUHP was recorded at 10 m/s. The sliding velocity corresponding to the lowest wear volume was 5 m/s for SN-GPLC and between 5 m/s and 10 m/s for SN-GPHE.

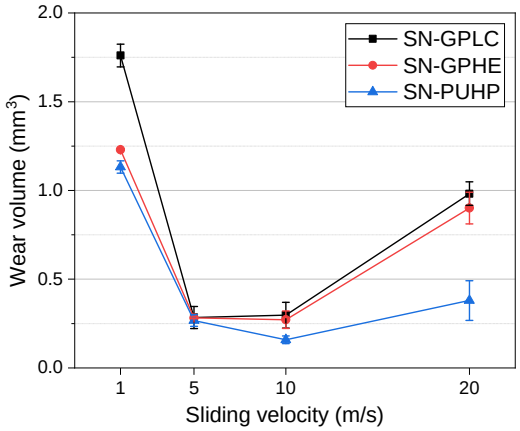


Fig. 5 Wear volume of the ceramics plotted against sliding velocity

## 3.2 Wear evolution of ceramics

### 3.2.1 Silicon nitride grade SN-GPLC

The wear surface morphology evolution of SN-GPLC is shown in Fig. 6. It can be seen from Fig. 6a and b that the surface of the ceramic is uneven, which is a typical feature of mechanical wear observed at

1 m/s and 5 m/s, respectively. Fig. 6c and d show that the wear surface becomes smooth at 10 m/s and 20 m/s. The other two ceramics (SN-GPHE and SN-PUHP) showed a similar wear behavior.

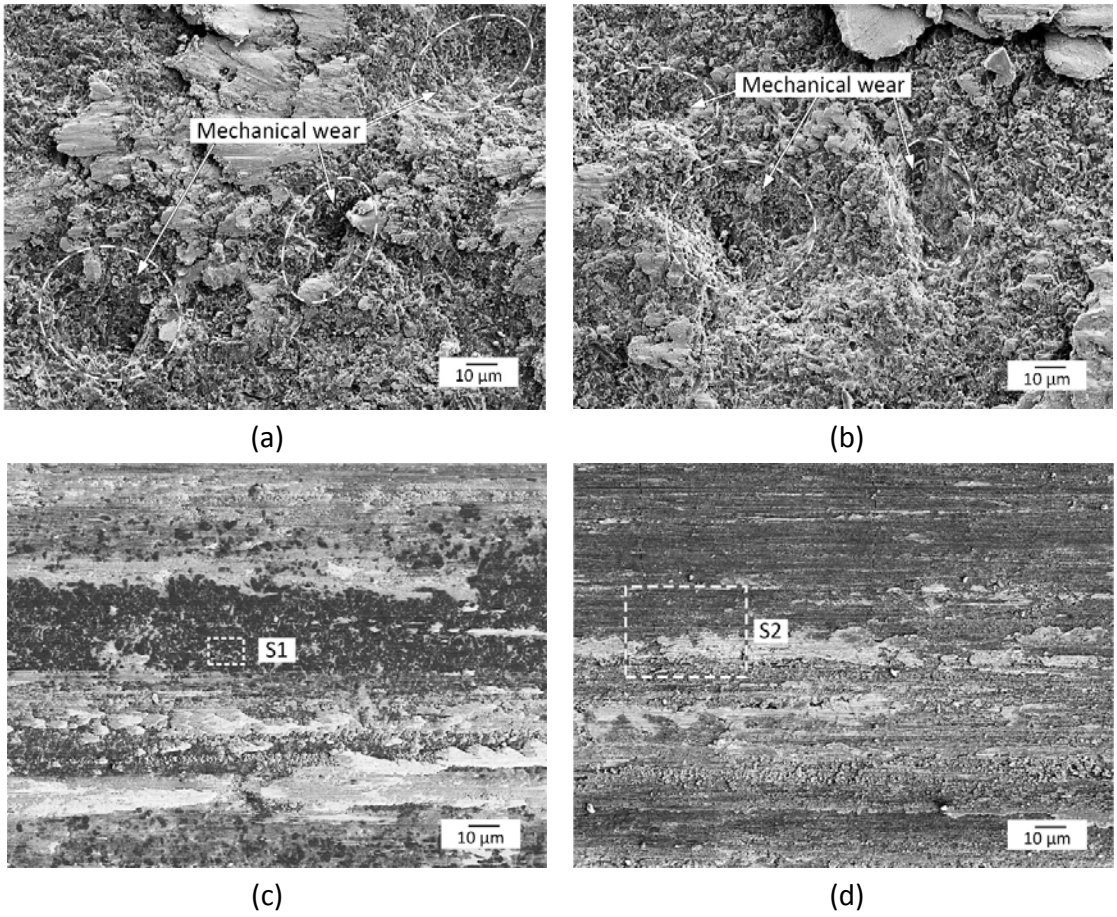


Fig. 6 Wear surfaces of SN-GPLC samples at sliding velocities of (a) 1 m/s, (b) 5 m/s, (c) 10 m/s, and (d) 20 m/s.

In order to study the wear surface at 10 m/s and 20 m/s in more detail, a magnified view of zone S1 (Fig. 6c) and zone S2 (Fig. 6d) are shown in Fig. 7. In Fig. 7a, the microstructure of the ceramic appears without signs of brittle fracture after running the test at 10 m/s. The structure of silicon nitride grains is relatively intact; however, the intergranular glassy phase underwent some changes to its morphology and no longer appears like the original glassy phase (see zone 7-a in Fig. 7a). The EDX analysis of zone 6-a resulted, in addition to Si and N, in 19.1 at.% O, 2.3 at.% Al and elements originally not found in the ceramic such as 7.2 at.% Cr, 1.5 at.% Nb, 1.1 at.% Ni and traces of Fe and Ti. At 20 m/s (shown in Fig. 7b), the wear surface shows cracks in addition to adhered Inconel 718 (light regions) and what appears to be plastically deformed material (dark regions such as zone 7-b). An EDX analysis of zone 7-b resulted in 42.7 at.% Si, 17.7 at.% N, 27.3 at.% O, 3.1 at.% Al, 4.2 at.% Cr, 2.9 at.% Ni, 1.2 at.% Fe, 0.5 at.% Ti and 0.7 at.% Nb.

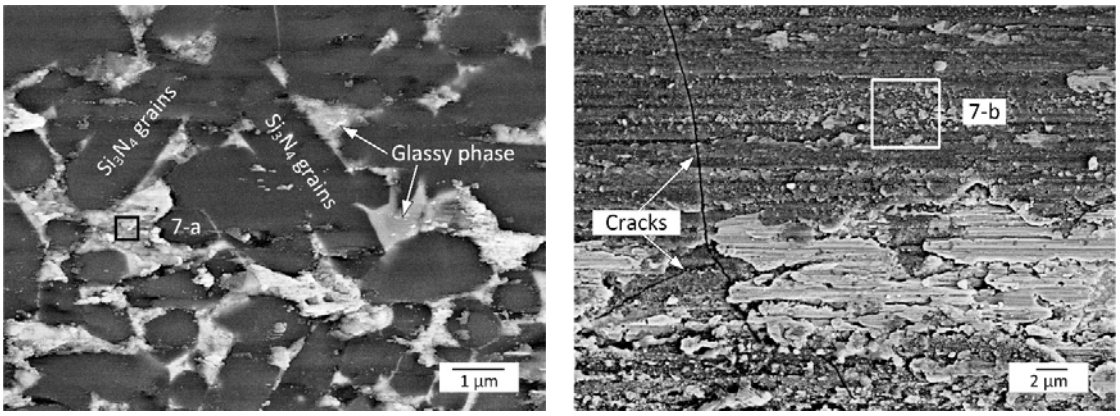


(a) (b)

Fig. 7 Magnified view of area (a) S1 and (b) S2 in Fig. 6c and d

SEM images of polished cross sections of SN-GPLC are shown in Fig. 8. At 10 m/s, a tribochemical layer appears between the ceramic and the Inconel 718 metallic transfer layer (buildup), see zone 8-a in Fig. 8a. At 20 m/s (Fig. 8b), there appears to be two transition zones (Q1 and Q2) between the ceramic and the metallic transfer layer. The substance in zone Q2 appears to react with the intergranular glassy phase as indicated by the small arrows. A bright phase also appears to diffuse into the grain boundary of SN-GPLC, see zone 8-b. Fig. 8a also shows microcrack, fracture of silicon nitride grains and grain refinement.

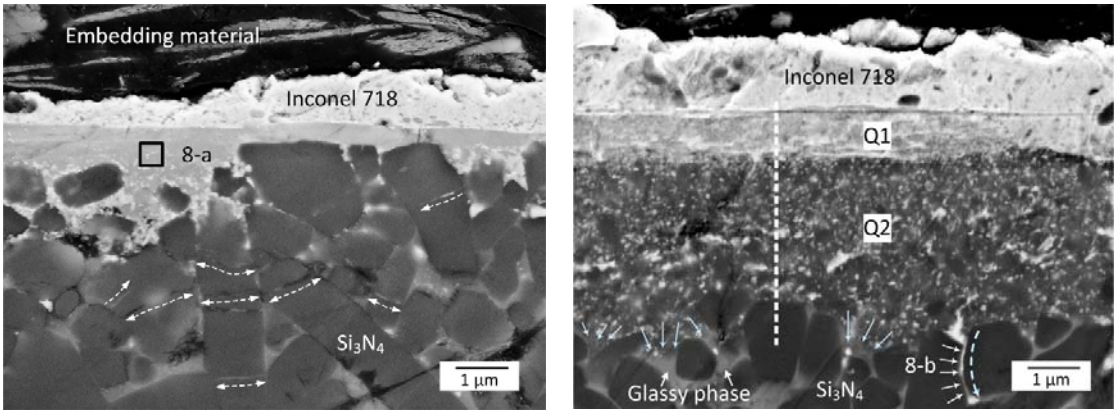


(a) (b)

Fig. 8 SEM image of a cross section of SN-GPLC at (a) 10 m/s and (b) 20 m/s

EDX line scan was conducted on zones Q1 and Q2 (Fig. 8b) as shown in Fig. 9. Zone Q1 is composed of high concentration of Ni, O, Cr, and Fe. Unlike zone Q2, no traces of N were detected in zone Q1. From zone Q1 towards zone Q2, the concentration gradient of the Inconel 718 elements (e.g., Ni, Cr and Fe) and of O is negative, while the concentration gradients of Si and N from are positive. Zone Q1 could be regarded as an oxide layer, and zone Q2 is more likely to be a diffusion layer (or combined diffusion-intermixing layer).

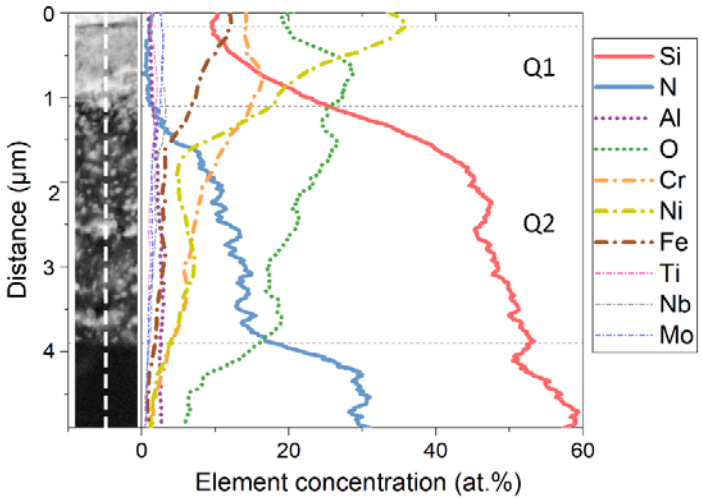


Fig. 9 EDX line analysis of the ceramic cross section in Fig. 8d (20 m/s)

Fig. 10 shows the element analysis of the zones indicated on the wear surface in Fig. 7 and the cross section in Fig. 8. Zone 8-a shows high concentration of Cr and O. By ignoring the Si and N signals obtained from zones 7-a and 8-a (assumed to be from the surrounding silicon nitride), the concentration ratios of the elements O, Cr, Al, Nb, Fe, and Ni appear to be similar in both regions (shown in 7-a* and 8-a* in Fig. 10). Zone 7-b on the wear surface is composed of 42.7 at.% Si, 17.6 at.% N, 27.3 at.% O, 3.0 at.% Al, 4.2 at.% Cr, 2.9 at.% Ni, 1.2 at.% Fe, and traces of Ti and Nb. This points out to its similarity to zone Q2 in the cross section. In addition to Si and N from silicon nitride, zone 8-b shows high concentration of O, in addition to Ni, Cr and Fe from Inconel 718.

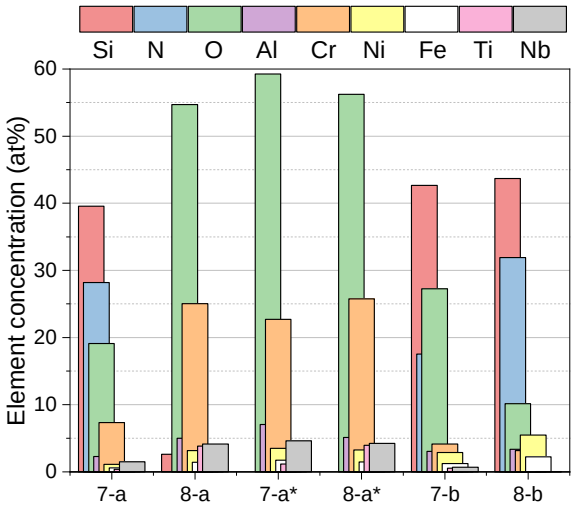


Fig. 10 EDX elemental analysis results of SN-GPLC ceramic (refer to Fig. 7 and Fig. 8)

### *3.2.2 Silicon nitride grade SN-GPHE*

Cross-sectional SEM of silicon nitride SN-GPHE at 10 m/s and 20 m/s are shown in Fig. 11. Similar to what has been observed in SN-GPLC, a tribochemical layer has initially formed between the ceramic and Inconel 718 buildup at 10 m/s (Fig. 11a). At 20 m/s, the tribochemical layer, the width of which appears slightly smaller than that of SN-GPLC, also consisted of two distinct regions: an oxide layer R1 and a diffusion layer R2 (Fig. 11b). Zone 11-b1 in Fig. 11b showed high concentrations of Ni (16.5 at.%), Fe (5.2 at.%) and Cr (3.5 at.%), in addition to Si and N from silicon nitride; it is comparable to zone 8-b in SN-GPLC.

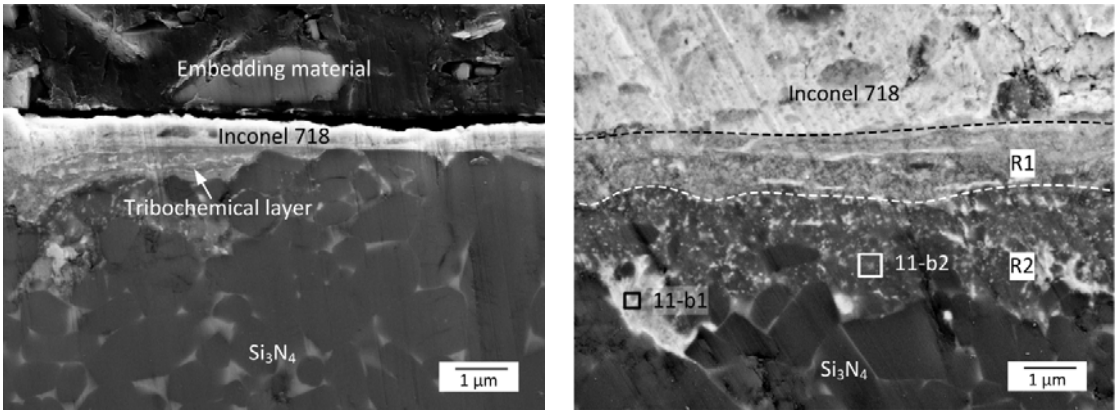


(a) (b)

Fig. 11 SEM image of a cross section of SN-GPHE at (a) 10 m/s and (b) 20 m/s

The typical surface morphology of SN-GPHE tested at 20 m/s is shown in Fig. 12. The surface exhibits fish-scale morphology in addition to tribochemical layer and adhered Inconel 718. The EDX results of zone 11-b2 and zone 12-a are compared in Fig. 13. These two zones contain elements both from silicon nitride and Inconel 718. Except for the slightly higher Si and O concentrations in zone 12-a, the element contents of these two zones are almost the same. This indicates that the fish-scale structure on the wear surface of SN-GPHE, which is slightly oxidized, corresponds to the diffusion zone R2 in the cross section shown in Fig. 11b.

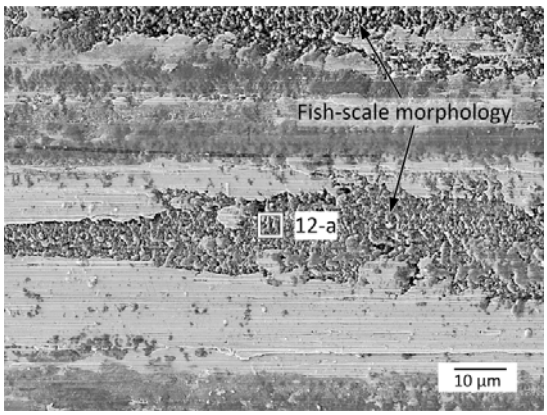


Fig. 12 Wear surface of SN-GPHE at 20 m/s

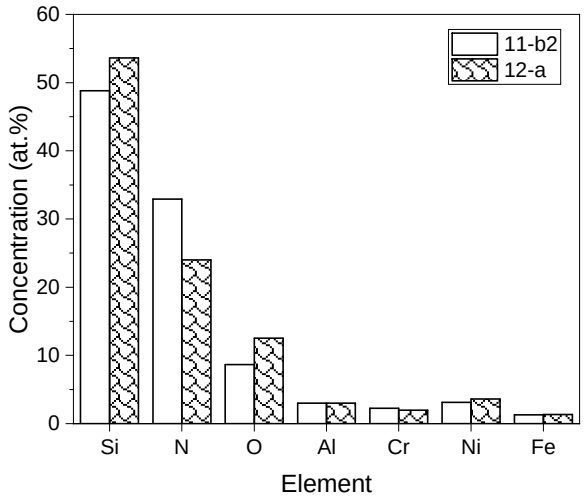


Fig. 13 EDX elemental analysis results of wear surface (12-a, Fig. 12) and cross section (11-b2, Fig. 11) of SN-GPHE ceramic

### *3.2.3 Silicon nitride grade SN-PUHP*

Unlike SN-GPLC and SN-GPHE, the interface between the ceramic and the metallic transfer layer in SN-PUHP at both 10 m/s and 20 m/s appears distinct and without the presence of a tribochemical layer (Fig. 14). At 20 m/s the metallic transfer layer contains dark patches (zone 14-b in Fig. 14b). The EDX results show that zone 11-b have high concentrations of O (41.9 at.%), Cr (28.9 at.%) and traces of Ni, Nb, Fe, Si, Al, and Ti.

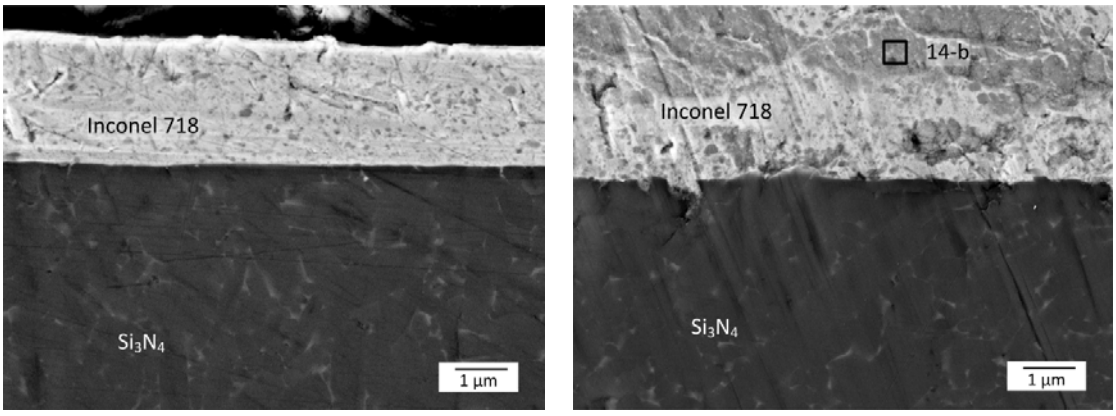


(a) (b)

Fig. 14 SEM image of a cross section of SN-PUHP at (a) 10 m/s and (b) 20 m/s

The typical wear surface morphology of SN-PUHP tested at 20 m/s is shown in Fig. 15. The wear surface is largely covered by thin layer (zone 15-a). EDX results of zone 15-a shows 48.4 at.% Si, 26.5 at.% N, 24.0 at.% O, and 1.1 at.% Al and no elements from Inconel 718, thus, indicating an oxide layer (mainly silicon oxide).

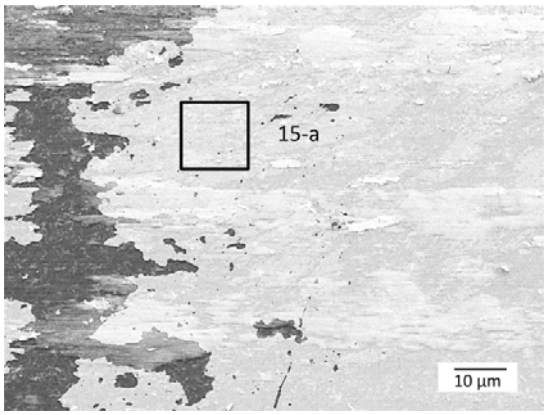


Fig. 15 Wear surface of SN-PUHP at 20 m/s

The SEM morphologies of wear debris generated during the tests using SN-GPLC and SN-PUHP at 20 m/s are shown in Fig. 16. The wear debris in testing SN-PUHP mainly consisted of Inconel 718 chips; whereas in the case of SN-GPLC, it was relatively small and difficult to distinguish between ceramic and metal debris based on its morphology. EDX analysis of zone 16-b1, shown in Fig. 17, indicated high concentrations of O, Si, Cr and Ni; similar to the oxide layer zone Q1 in Fig. 8. Zone 16-b2 contains higher N and Si and lower concentrations of O and Inconel 718 elements in comparison to zone 16-b1, the former of which is similar to the diffusion layer zone Q2 in Fig. 8.

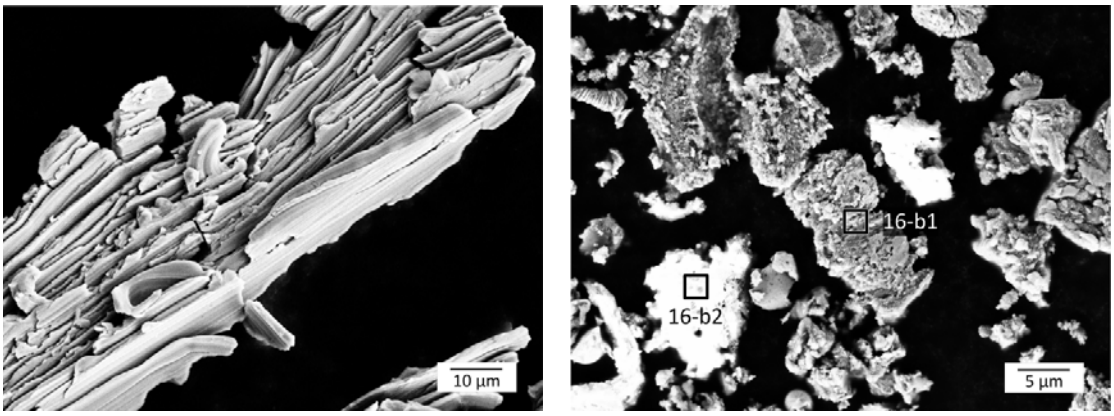


(a) (b)

Fig. 16 SEM morphology of wear debris generated at 20 m/s for (a) SN-PUHP and (b) SN-GPLC

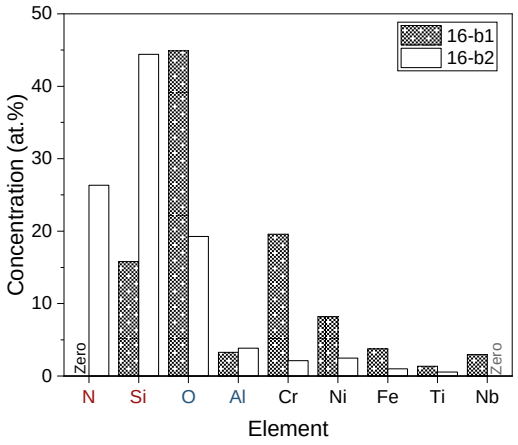


Fig. 17 EDX elemental analysis of wear debris (Fig. 16b) of SN-GPLC ceramic

# 4 Discussion

Three fully-dense silicon nitride ceramics with different microstructural and mechanical properties showed different tribological behavior over a wide range of velocities. Even though the COF at the same sliding velocity was almost the same, the wear rates of the different ceramics showed considerable disparity. Similar phenomena were also found by Kumar et al. [19] and Campbell et al. [20] in studying wear of different SiAlON ceramics sliding against ceramics and metals, respectively. The authors found no clear correlation between the COF and microstructural features. Referring to Fig. 5, the wear resistance of the three ceramics was as follows: SN-PUHP > SN-GPHE > SN-GPLC. The range of optimum sliding velocity corresponding to lowest wear was found in the rage between 5 m/s and 10 m/s.

## 4.1 Mechanical wear mechanism at low velocities

At 1 m/s, the wear mechanism is mainly mechanical wear, which is generally accepted to be related to the hardness and fracture toughness of the ceramic [21]. Based on the lateral crack model of ceramic wear proposed by Evans [7], the wear resistance $K_{IC}^{3/4} \cdot H_V^{1/2}$ of the three ceramics calculated from the data listed in Table 1 should be as follows: SN-GPHE > SN-PUHP > SN-GPLC. As shown in Fig. 18, the experimental wear resistance of the three ceramics at 1 m/s increases with increasing Vickers hardness; thus, does not match the trend predicted by the aforementioned model. The wear of the three silicon nitride ceramics has a strong positive correlation with hardness at 1 m/s. This finding is consistent with the tensile crack wear model proposed by Wang et al. [22]. It can be safely assumed that the hot-hardness scales with the high-temperature strength of the three ceramics (refer to Fig. 1a) and hence, follows the same trend with SN-GPLC having the lowest value and SN-PUHP the highest. Mutoh et al. [23] found that the fracture toughness of silicon nitride does not change up to a temperature of 800 °C, which corresponds to the glass transition point.

On the other hand, a lower content of intergranular glassy phase tends to decrease tensile residual stresses at the $Si_3N_4$ grain boundaries [24], which would also improve wear resistance [25]. Moreover, it was shown that the refinement of grain size should have a positive effect on wear [11, 26]. Nonetheless, as shown in Fig. 5, the wear volumes measured for SN-GPHE and SN-PUHP at 1 m/s are very close; even though the typical crystal length in SN-GPHE is almost four times shorter than that in SN-PUHP (Table 2). Moreover, the hardness of SN-PUHP did not show significant improvement despite its finer grain structure. Therefore, it can be concluded that grain refinement did not have any significant impact on wear reduction in this particular case. Less grain boundary phase (Fig. 2) and higher hardness (Table 1) are thought to be the main reasons behind the improved wear resistance of SN-PUHP at 1 m/s.

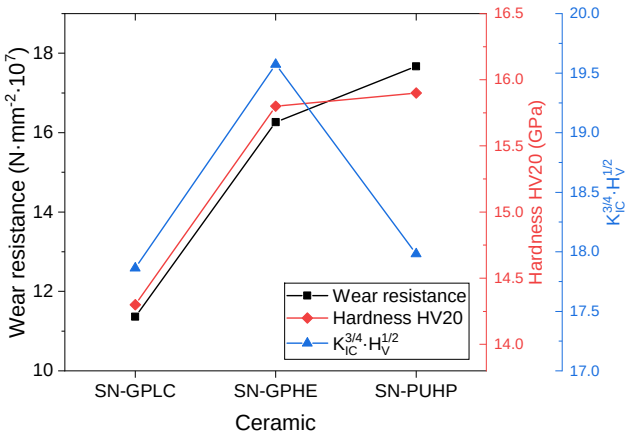


Fig. 18 Wear resistance of ceramics at a sliding velocity of 1 m/s

The wear rate of the three ceramics at 5 m/s was almost identical. As shown in Fig. 6b, the morphology of the wear surfaces at 5 m/s is similar to that at 1 m/s; hence, it can be safely assumed that the wear mechanism is somewhat similar within this velocity range. With increasing sliding velocities, the contact temperature increases due to increasing frictional power. Based on a model developed by Zhao et al. [27], a ceramic contact surface temperature exceeding 1000 °C was estimated. Such high temperatures would eliminate tensile residual stresses at the grain boundaries and thus, decrease hardness [28]. In addition, it was found that the disparity in hardness between ceramic materials with different intergranular glassy phase contents becomes smaller at temperatures around 1000 °C [29, 30]. Consequently, the wear volume of the tested ceramics at 5 m/s becomes closer as residual stresses are released and the difference in hardness becomes smaller.

## 4.2 Tribochemical wear mechanism at high velocity

At velocities of 10 m/s and 20 m/s, SN-GPLC and SN-GPHE underwent similar tribochemical wear. This was confirmed through the cross-sectional analysis shown in Fig. 8 and Fig. 11. At 10 m/s, a thin

tribochemical layer initially formed at the interface between the ceramic and the metallic transfer layer, see Fig. 8a and Fig. 11a. Previous studies have documented the observation of similar layers when studying different silicon nitride materials in sliding contact against Inconel 718 at room temperature [17] and high temperature [27]. The tribochemical layer can be detached from the ceramic surface by shearing during the frictional process, thus, exposing the microstructure of the ceramic as shown in Fig. 7a. With the sliding velocity increasing to 20 m/s, the contact temperature increases, hence, promoting the formation of a thick diffusion layer at the interface (zone Q2 in Fig. 8b and zone R2 in Fig. 11b). The EDX analysis of zone 7-b in Fig. 7b and zone 12-a in Fig. 12 indicates that the wear surfaces of SN-GPLC and SN-GPHE have a chemical composition similar to that of the diffusion layer. This indicates that the removal of material occurs within the diffusion layer and points out to its low shear strength. The composition of wear debris in testing SN-GPLC (Fig. 16b) appears to be similar to that of the oxide and diffusion layers, which confirms the detachment of these layers. Therefore, in comparison with the thinner tribochemical layers formed at 10 m/s, thicker diffusion layers result in higher wear rates of ceramics at 20 m/s.

As shown in Fig. 10, high concentrations of Cr and O were detected in zone 8-a, which indicate an oxidational process of Inconel 718 at 10 m/s. For this velocity, the difference in the COF for all three ceramics was very small (Fig. 4) and hence, the difference in frictional power. As shown in Fig. 1b, the thermal conductivity and specific heat of SN-PUHP are the highest among all three ceramics. The contact temperature of SN-PUHP is speculated to be the lowest and not high enough to cause oxidation of Inconel 718 at 10 m/s. It can be seen from Fig. 7a and Fig. 8a that the intergranular glassy phase near the wear surface dissolves into the tribochemical layer at 10 m/s. The selective degradation of the intergranular glassy phase may start occurring at a much lower temperature depending on the composition. The silicon nitride grains also underwent degradation at 10 m/s (Fig. 8), which is believed to have been caused by excessive high thermal loading and mechanical stresses. Once the intergranular glassy phase has undergone enough degradation, fragmentation of silicon nitride grains intensifies chemical interactions with Inconel 718 and atmospheric oxygen. At 20 m/s, by referring to the elements distribution within the tribochemical layer given in Fig. 9, it becomes clear that the elements from the oxide layer diffuse into (and intermix with) silicon nitride to form a diffusion layer. Although the EDX profile appears to be gradually changing from one phase to another, the transition may actually be rather abrupt; however, such spatial detection is limited by the EDX capabilities. Zone 8-b in Fig. 8b and zone 11-b1 in Fig. 11b both contain high concentrations of O, Ni, Cr and Fe elements. Thus, the formation of the diffusion layer occurs due to the diffusion of O, Ni, Cr and Fe into the intergranular glassy phase and fragmentation of silicon nitride grains.

As shown in Fig. 14b in testing SN-PUHP at 20 m/s, no tribochemical layer was observed at the interface between the ceramic and the metallic transfer layer; Cr-O-rich regions formed within the Inconel 718 transfer layer (buildup). In Fig. 15, the wear surface of SN-PUHP tested at 20 m/s is shown to have been oxidized into silicon oxide. A plausible explanation would be traced back to the intergranular glassy phase content in SN-PUHP that may be too scarce to form a tribochemical layer even though the contact temperature is high enough to oxidize both silicon nitride and Inconel 718. In addition, the thicker tribochemical layer observed in SN-GPLC, which has a higher content of intergranular glassy phase (Fig. 8) in comparison to SN-GPHE (Fig. 11), confirms this hypothesis. It should be noted that the composition of the intergranular glassy phase plays a crucial role in the formation of tribochemical layers; in this particular case the sintering additives in all three ceramics were similar. Related results were also reported by Campbell et al. in studying the tribology of SiAlONs in contact with iron-based alloys [31]. SN-PUHP with the least amount of intergranular glassy phase exhibits the best wear resistance at 10 m/s and 20 m/s.

The formation mechanism of tribochemical layer can be described as follows:

- Phase I: At low velocities (≤ 5 m/s), the wear mechanism of the ceramics is mainly mechanical wear; tribochemical reactions are not detected. At 10 m/s, high contact temperature oxidizes Inconel 718 to form Cr-O-rich zones (Fig. 14b).
- Phase II: the Cr-O-rich zones interact selectively with the intergranular glassy phase of silicon nitride to form an oxidation layer (Fig. 8a and Fig. 11a). If the amount of the intergranular glassy phase is not enough to form this layer, the Cr-O-rich zones would remain within the Inconel 718 buildup (occurs in SN-PUHP as shown in Fig. 14b). Otherwise, the surface-near microstructure of silicon nitride would be compromised and the newly formed oxidation layer can be easily detached, leading to higher wear of the ceramic (occurs in SN-GPLC as shown in Fig. 8a).
- Phase III: with increasing contact temperature, the fragmentation of silicon nitride grains takes place and the elements from the oxidation layer formed in phase II diffuse into and intermixed with degraded silicon nitride to form a thick diffusion layer (occurs in SN-GPLC as shown in Fig. 8b and in SN-GPHE as shown in Fig. 11b). Due to shear forces, the progressive wear of ceramic occurs mainly within the diffusion layer, thus, accelerating the wear of the material.

## Conclusions

The tribological behavior of three silicon nitride ceramics was investigated under dry sliding contact against Inconel 718 from 1 m/s to 20 m/s. The analysis of wear was studied by means of pin-on-disk

experiments. The mechanical and microstructural properties of the ceramics were considered in the wear mechanism analysis. The following points can be concluded:

- The COF of all three ceramics decreased with increasing sliding velocities; the difference in COF values was very small. The wear volume showed a decrease up to a certain velocity after which is increased. The optimal sliding velocity corresponding to the lowest wear volume was 5 m/s for SN-GPLC, between 5 and 10 m/s for SN-GPHE and 10 m/s for SN-PUHP. SN-PUHP shows the best wear resistance over the entire speed range.
- At low velocities of 1 m/s to 5 m/s, the wear of the ceramics was predominantly mechanical wear. It showed direct correlation with the hardness of ceramic. Less intergranular glassy phase content also showed preferential wear behavior. The grain size did not have a significant effect on the wear resistance of the material.
- At high velocities of 10 m/s to 20 m/s, tribochemical wear becomes dominant and leads to higher wear rates. The formation of a tribochemical layer was caused by the oxidation of Inconel 718 and diffusion into the intergranular glassy phase of silicon nitride. The amount of intergranular glassy phase played a decisive role in the formation of the tribochemical layer. SN-PUHP with the least amount of intergranular glassy phase showed the best tribochemical wear resistance.
- It is recommended to use silicon nitride ceramics with low content of intergranular glassy phase in high-speed friction process.

## Acknowledgements

This work has received funding from the Sino-German (CSC-DAAD) Postdoc Scholarship Program 2018 [57395819] supported by China Scholarship Council (CSC) and the German Academic Exchange Service (DAAD) in addition to partial funding from the European Union's RFCS under grant agreement no. 709920 "ReduWearGuid".

## References

[1] D. Dudzinski, A. Devillez, A. Moufki, D. Larrouquère, V. Zerrouki and J. Vigneau, "A review of developments towards dry and high speed machining of Inconel 718 alloy," *International Journal of Machine Tools and Manufacture,* vol. 44, no. 4, pp. 439-456, 2004.

[2] J. Zhao, X. Ai and Z. Lü, "Preparation and characterization of Si3N4/TiC nanocomposite ceramics," *Materials Letters,* vol. 60, no. 23, pp. 2810-2813, 2006.

[3] B. Zou, C. Huang, M. Chen, M. Gu and H. Liu, "Study of the mechanical properties, toughening and strengthening mechanisms of $Si_3N_4$/$Si_3N_{4w}$/TiN nanocomposite ceramic tool materials," *Acta Materialia,* vol. 55, no. 12, pp. 4193-4202, 2007.

[4] X. Tian, J. Zhao, H. Yang, Z. Wang and H. Liu, "High-speed intermittent turning of GH2132 alloy with $Si_3N_4$/(W, Ti)C/Co graded ceramic tool," *The International Journal of Advanced Manufacturing Technology,* vol. 100, no. 1-4, pp. 401-408, 2019.

[5] R. P. Zeilmann, F. Fontanive and R. M. Soares, "Wear mechanisms during dry and wet turning of Inconel 718 with ceramic tools," *The International Journal of Advanced Manufacturing Technology,* vol. 92, no. 5-8, pp. 2705-2714, 2017.

[6] J. Deng and X. Ai, "Wear behavior and mechanisms of alumina-based ceramic tools in machining of ferrous and non-ferrous alloys," *Tribology International,* vol. 30, no. 11, pp. 807-813, 1997.

[7] A. G. Evans and T. R. Wilshaw, "Quasi-static solid particle damage in brittle solids—I. Observations analysis and implications," *Acta Metallurgica,* vol. 24, no. 10, pp. 939-956, 1976.

[8] A. S. Kumar, A. R. Durai and T. Sornakumar, "Wear behaviour of alumina based ceramic cutting tools on machining steels," *Tribology International,* vol. 39, no. 3, pp. 191-197, 2006.

[9] C. P. Doğan and J. A. Hawk, "Influence of whisker toughening and microstructure on the wear behavior of $Si_3N_4$- and $Al_2O_3$-matrix composites reinforced with SiC," *Journal of Materials Science,* vol. 35, no. 23, pp. 5793-5807, 2000.

[10] D. S. Park, B. D. Han, D. S. Lim and I. W. Yeo, "A study on wear and erosion of sialon-Si3N4 whisker ceramic composites," *Wear,* Vols. 203-204, p. 284, 1997.

[11] G. d. Portu and S. Guicciardi, "Wear of Hard Ceramics," in *Comprehensive Hard Materials*, Elsevier, 2014, pp. 385-412.

[12] S. Kurama, I. Schulz and M. Herrmann, "Wear properties of α- and α/β-SiAlON ceramics obtained by gas pressure sintering and spark plasma sintering," *Journal of the European Ceramic Society,* vol. 31, no. 5, pp. 921-930, 2011.

[13] N. Narutaki, Y. Yamane, K. Hayashi, T. Kitagawa and K. Uehara, "High-speed machining of Inconel 718 with ceramic tools," *CIRP Annals,* vol. 42, no. 1, pp. 103-106, 1993.

[14] S. K. Bhattacharyya, A. Jawaid, M. H. Lewis and J. Wallbank, "Wear mechanisms of Syalon ceramic tools when machining nickel-based materials," *Metals Technology,* vol. 10, no. 1, pp. 482-489, 1983.

[15] H. Addhoum and D. Broussaud, "Interaction of ceramic cutting tools with nickel-based alloys," *Materials Science and Engineering: A,* vol. 109, pp. 379-387, 1989.

[16] A. Renz, I. Khader and A. Kailer, "Tribochemical wear of cutting-tool ceramics in sliding contact against a nickel-base alloy," *Journal of the European Ceramic Society,* vol. 36, no. 3, pp. 705-717, 2016.

[17] I. Khader, A. Renz and A. Kailer, "A wear model for silicon nitride in dry sliding contact against a nickel-base alloy," *Wear,* Vols. 376-377, pp. 352-362, 2017.

[18] "INCONEL® Alloy 718," Special Metals Corporation, September 2007. [Online]. Available: http://www.specialmetals.com.

[19] R. Kumar, N. C. Acikbas, F. Kara, H. Mandal and B. Basu, "Microstructure–Mechanical Properties–Wear Resistance Relationship of SiAlON Ceramics," *Metallurgical and Materials Transactions A,* vol. 40, no. 10, pp. 2319-2332, 2009.

[20] P. Campbell, T. Laoui, J. P. Celis and O. Van Der Biest, "The influence of intergranular phases on the tribological performance of sialons," *Materials Science and Engineering: A,* vol. 207, no. 1, pp. 72-86, 1996.

[21] S. M. Hsu and M. Shen, "Wear prediction of ceramics," *Wear,* vol. 256, no. 9-10, pp. 867-878, 2004.

[22] Y. Wang and S. M. Hsu, "Wear and wear transition modeling of ceramics," *Wear,* vol. 195, no. 1-2, pp. 35-46, 1996.

[23] Y. Mutoh, N. Miyahara, K. Yamaishi and T. Oikawa, "High temperature fracture toughness in silicon nitride and sialon," *Journal of Engineering Materials and Technology,* vol. 115, no. 3, pp. 268-272, 1993.

[24] I. M. Peterson and T. Y. Tien, "Effect of the grain boundary thermal expansion coefficient on the fracture toughness in silicon nitride," *Journal of The American Ceramic Society,* vol. 78, no. 9, pp. 2345-2352, 1995.

[25] B. Lawn, Fracture of brittle solids, Cambridge: Cambridge University Press, 1993.

[26] C. P. Doğan and J. A. Hawk, "Microstructure and abrasive wear in silicon nitride ceramics," *Wear,* vol. 250, no. 1-12, pp. 256-263, 2001.

[27] B. Zhao, I. Khader, R. Raga, G. Konrath, U. Degenhardt and A. Kailer, "High temperature tribological properties of silicon nitride in dry sliding contact against Inconel 718 heated by laser," *Wear,* Vols. 434-435, p. 203000, 2019.

[28] B. Zhao, H. Liu, C. Huang, J. Wang, M. Cheng and Q. Zhan, "Evolution mechanisms of high temperature mechanical properties and microstructures of $Al_2O_3/SiC_w/TiC_n$ nanocomposite materials," *Journal of Alloys and Compounds,* vol. 737, no. 15, pp. 46-52, 2018.

[29] R. F. Silva and J. M. Vieira, "Hot hardness of $Si_3N_4$-based materials," *Journal of Materials Science,* vol. 30, no. 21, pp. 5531-5536, 1995.

[30] C. P. Alpert, H. M. Chan, S. J. Bennison and B. Lawn, "Temperature dependence of hardness of alumina-based ceramics," *Journal of the American Ceramic Society,* vol. 71, no. 8, pp. C-371-C-373, 1988.

[31] P. Campbell, L. T., J. P. Celis and O. Van Der Biest, "The influence of intergranular phases on the tribological performance of sialons," *Materials Science and Engineering: A,* vol. 207, no. 1, pp. 72-86, 1996.